Generation and evolution of spin-, valley- and layer-polarized excited carriers in inversion-symmetric WSe$_2$

Roman Bertoni[1‡], Christopher W. Nicholson[1], Lutz Waldecker[1], Hannes Hübener[2], Claude Monney[3], Umberto De Giovannini[2], Michele Puppin[1], Moritz Hoesch[4], Emma Springate[5], Richard T. Chapman[5], Cephise Cacho[5], Martin Wolf[1], Angel Rubio[2,6] and Ralph Ernstorfer[1]*

1 Fritz Haber Institute of the Max Planck Society, Faradayweg 4-6, 14195 Berlin, Germany
2 Nano-Bio Spectroscopy Group and ETSF, Universidad del País Vasco, CFM CSIC-UPV/EHU, 20018 San Sebastian, Spain
3 University of Zurich, Department of Physics, Winterthurerstrasse 190, 8057 Zürich, Switzerland
4 Diamond Light Source, Harwell Campus, Didcot OX11 0DE, United Kingdom
5 Central Laser Facility, STFC Rutherford Appleton Laboratory, Harwell Campus, Didcot OX11 0QX, United Kingdom
6 Max Planck Institute for the Structure and Dynamics of Matter and Center for Free-Electron Laser Science,
  Notkestraße 85, 22761 Hamburg, Germany
‡current address: Université de Rennes 1, Institut de Physique de Rennes, UMR UR1-CNRS 6251, Rennes, France
e-mail: ernstorfer@fhi-berlin.mpg.de

Manipulation of spin and valley degrees of freedom is a key step towards realizing novel quantum technologies[1–4], for which atomically thin transition metal dichalcogenides (TMDCs) have been established as promising candidates. In monolayer TMDCs, the lack of inversion symmetry gives rise to a spin-valley correlation of the band structure allowing for valley-selective electronic excitation with circularly polarized light[5,6]. Here we show that, even in centrosymmetric samples of 2H-WSe$_2$, circularly polarized light can generate spin-, valley- and layer-polarized excited states in the conduction band. Employing time- and angle-resolved photoemission spectroscopy (trARPES) with spin-selective excitation, the dynamics of valley and layer pseudospins of the excited carriers are investigated. Complementary time-dependent density functional theory (TDDFT) calculations of the excited state populations reveal a strong circular dichroism of the spin-, valley- and layer-polarizations and a pronounced 2D character of the excited states in the K valleys. We observe scattering of carriers towards the global minimum of the conduction band on a sub-100 femtosecond timescale to states with three-dimensional character facilitating inter-layer charge transfer. Our results establish the optical control of coupled spin-, valley- and layer-polarized states in centrosymmetric materials and suggest the suitability of TMDC multilayer materials for valleytronic and spintronic device concepts.

Semiconducting TMDCs are materials consisting of stacked layers of two-dimensional (2D) sheets. While their overall crystal structure is inversion symmetric, individual layers lack this property. The missing inversion symmetry of isolated monolayers, in combination with strong spin-orbit coupling of TMDCs[5] lifts the energy degeneracy of electronic bands of opposite spin polarizations. Valley selective excitation of spin-polarized electrons is achieved by applying circularly polarized light[1,2,6–8]. Hence atomically thin TMDCs have been identified as a playground for controlling the spin and valley degrees of freedom. Recent theoretical work suggests that the absence of inversion symmetry within moieties of the unit cell, which has been phrased atomic site asymmetry, locally lifts the spin degeneracy[9]. The lack of inversion symmetry and the presence of in-plane dipole moments within individual TMDC trilayers can be seen as atomic site Dresselhaus and Rashba effects and cause a hidden spin texture in a globally inversion symmetric material[9]. This is supported by the observation of spin-polarized valence bands in 2H-WSe$_2$ by photoelectron spectroscopy[10]. A more recent spin-resolved ARPES study by Riley et al. provides a momentum-resolved view of the spin texture in the valence bands of this material[11]. Photoluminescence experiments on inversion symmetric samples, however, do not show signatures of spin and valley polarization[1,2], suggesting that selective excitation of electrons in the spin-valley-layer-coupled band structure of centrosymmetric TMDCs would not be possible.

In this work, we demonstrate the selective excitation of electrons in bulk 2H-WSe$_2$ into different electronic valleys by means of optical excitation with circularly polarized light. TDDFT calculations[12] confirm the valley- and layer-selectivity of the different pump polarizations and reveal the underlying excited state electronic structure. We additionally identify scattering pathways in momentum space and determine time constants of electronic lifetimes in the valleys of the conduction band, which is of central importance for conceiving devices based on multilayers or heterostructures of TMDCs. Our measurements reveal the rapid transfer of the initial population at the corner (K points) of the Brillouin Zone (BZ) to the global minimum of the conduction band at the Σ points, where the interlayer coupling is strongly enhanced.
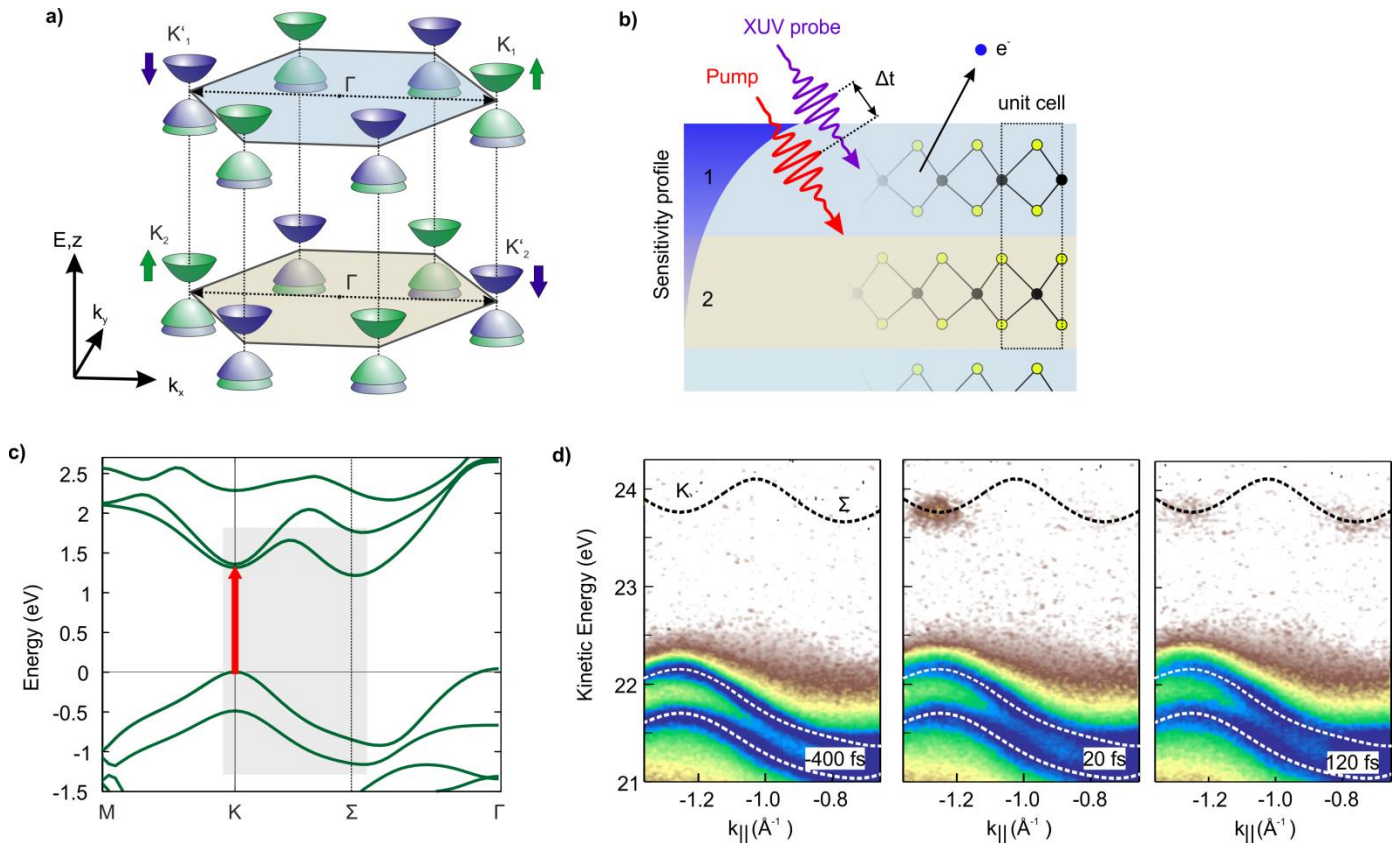

FIGURE 1. Valley- and layer-selective time-resolved photoelectron spectroscopy of WSe$_2$. **a)** Sketch of the local band structure and the spin-valley correlation at the K and K' points of two non-interacting layers with 2H stacking. The two layers together comprise the Brillouin zone of both bilayer and bulk crystal, in which the spin-polarization vanishes for every **k**-point. **b)** Depiction of the trARPES configuration probing half of the BZ. Pump-pulses excite the sample and XUV probe pulses emit electrons. Sensitivity to the top layer is given by the short mean free path of electrons within the material. **c)** Electronic band structures of bilayer WSe$_2$ calculated by DFT. The red arrow and the shaded rectangle indicate the optical excitation and the experimentally investigated part of the electronic structure, respectively. **d)** Electron intensity maps at various pump-probe delays obtained with linearly polarized pump pulses (logarithmic colour scale). The kinetic energy scale has been corrected for the analyser work function. The overlaid bands are of the bilayer DFT calculations, with the conduction bands shifted 400 meV upwards to match the experimental observations.

The electronic bands and the corresponding spin polarizations at the K points of two decoupled layers of WSe$_2$ with 2H stacking are depicted in Figure 1a. As the valence states in the K valleys are well localized within the atomic layers[11,13], it is possible to relate spin-polarized valleys to individual layers[14]. The integrated spin-polarization, however, vanishes for every **k**-point due to the inversion symmetry of the unit cell. The band structure of an inversion-symmetric bilayer of WSe$_2$, as calculated by DFT (see Methods for details), is shown in Figure 1c. The global minimum of the conduction band Σ is located about halfway between Γ and K, in agreement with previous work[13,15].

We employ trARPES with femtosecond extreme ultraviolet (EUV) probe pulses of 23 eV photon energy (see Methods) in order to probe the response of the electronic structure to optical excitation along the Σ-K and Σ'-K'

lines in the BZ within an energy window including the spin-split valence bands and the lowest conduction bands. With this photon energy, the mean free path of photo-emitted electrons is shorter than one layer, resulting in a very high surface sensitivity[11]. This allows experimental access to the electron dynamics in the top layer, i.e. the upper half of the topmost unit cell of the sample, as illustrated in Figure 1b. In combination with spin-selective excitation, our experimental approach therefore provides spin-, valley- and layer-resolved information of the excited state population. The pump pulses are tuned into resonance with the A exciton absorption at 1.63 eV[16], corresponding to direct optical transitions at the K point, as indicated by the red arrow in Figure 1c. The applied fluences are on the order of few mJ/cm^2 and result in excitation densities above the threshold for the excitonic Mott transition[17], therefore creating an electron-hole plasma. Three representative photoelectron intensity maps of WSe$_2$ obtained using linearly polarized pump-pulses are shown in Figure 1d. The map has been overlaid with the calculated band structure of the bilayer, indicating the position of the conduction band valleys at K and Σ, which are initially unoccupied. Upon optical excitation, states at the K point are resonantly excited and this population is transferred to the Σ valleys at longer delay times, as shown in the third panel.
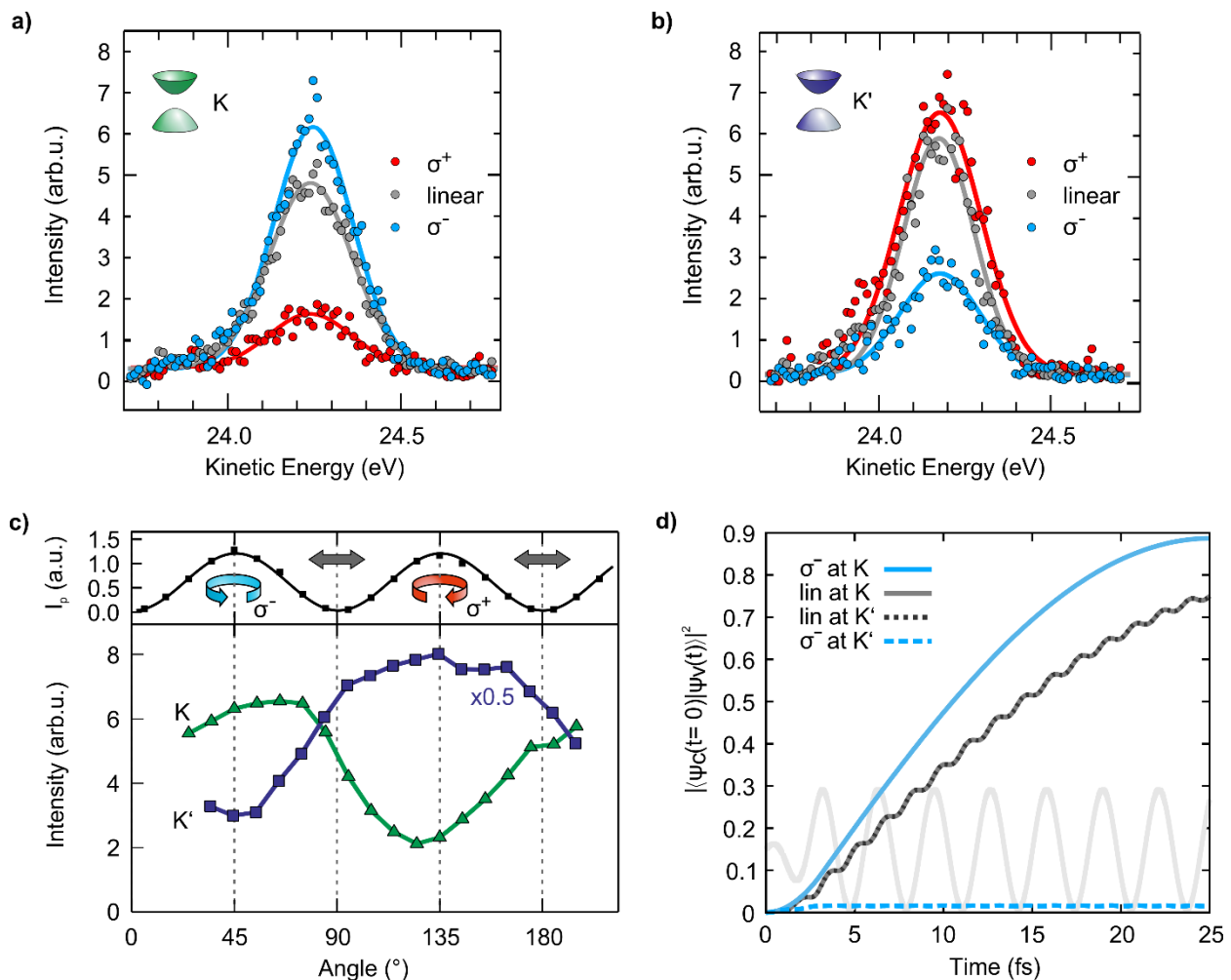

FIGURE 2. Circular dichroism of valley- and layer-resolved excited state population. a,b) Energy distribution curves of the excited state signal at K and K', 15 fs after excitation with optical pump pulses of different polarizations. **c)** Excited state photoelectron intensity at the K point (green triangles) and the K' point (blue squares) at a fixed pump-probe delay as a function of the angle of a quarter-wave plate in the pump beam. The upper panel shows the measurement (squares) and fit (lines) of the parallel component of the pump polarization, from which the polarization state in dependence of the wave plate angle is deduced. **d)** Evolution of excited state population at the K and K' points in the upper half of a WSe$_2$ bilayer for linear and circular (σ$^-$) pump polarization from TDDFT simulations. While linear polarization results in the same excited state build-up at K and K', optical excitation with circular polarized light results in spin-valley-locked excited states localized on individual tri-layers with a high degree of valley polarization. Opposite helicity inverts the valley polarization (not shown). The light grey oscillation indicates the applied electric field of the simulation.

We now monitor the excited state population in the K valleys after excitation with circularly polarized light. The energy distribution curves (EDCs) of the conduction band at the K point, taken at a delay of $\Delta t = 15$ fs, are presented in Figure 2a for excitation with light of both circular helicities and of linear polarization. A strong circular dichroic effect is evident in the excited state population with σ^+ light exciting significantly more electrons in the K valley compared to σ^-, and excitation with linear polarization being intermediate. The excited state population in the non-equivalent K' valley shows the opposite effect with respect to helicity, see Figure 2b. The continuous evolution of excited state populations in the K and K' valleys in dependence of the polarization state is shown in Figure 2c, showing an oscillatory dependence of the excited state signal on the angle of a quarter-wave plate, which gradually changes the polarization of the pump pulses from circular left to linear p-polarised to circular right as indicated by the arrows. The minima and maxima of the excited state population occur at angles corresponding to circular polarizations, and maximal excitation at the two inequivalent K points occurs for opposite helicity.

Figure 2d shows the simulated evolution of the valence states of the upper layer of bilayer WSe_2 under different pump polarizations (see Methods). Whereas linear polarized light results in a build-up of excited state population at both K and K' points, we observe a pronounced dichroism of the layer-projected excited state population at the corners of the BZ for circular polarization. We confirmed that this population build-up is also visible in an *ab initio* simulation of the pump-probe ARPES process. The experiments together with the TDDFT calculations unambiguously demonstrate the ability to valley- and spin-selectively excite electrons in bulk 2H-WSe_2, additionally leading to a layer-pseudospin polarization.
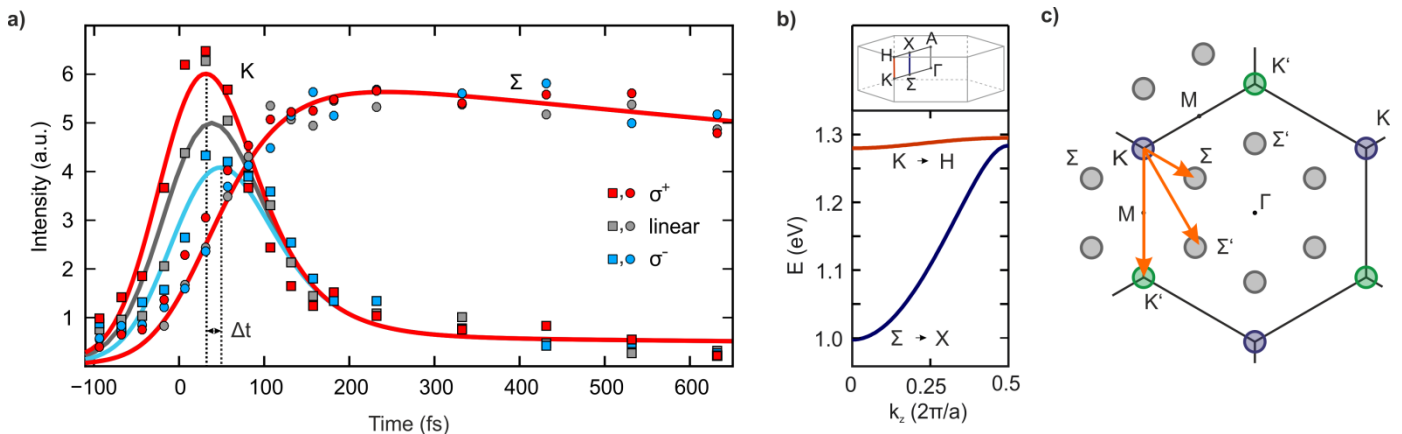

FIGURE 3. Intervalley scattering and electronic relaxation. a) Temporal evolution of photoelectron intensity in the conduction band at K (squares) and Σ (circles) for different pump polarizations. A small delay of intensity for σ^- indicates that electronic scattering decreases the observed dichroism. Different initial populations at K do not translate into significant differences in population at Σ. The solid lines are taken from a scattering model (see text). **b)** Top: sketch of the BZ of bulk WSe_2. Bottom: Dispersion of the conduction band states in bulk WSe_2 along the K-H and Σ-X directions as defined above. States at K are strongly localized within the layers in real-space, whereas states at Σ have a more three-dimensional character. **c)** Top-view onto upper half of the Brillouin zone including K and Σ valleys. The orange arrows indicate possible electronic scattering processes between the valleys.

The measured dichroic contrast at the K-points (Figure 2) critically depends on pump-probe delay and diminishes at long delay times. The temporal evolution of the photoelectron intensity in the conduction band is shown in Figure 3a for σ^+, linear and σ^- pump polarizations. In the K valleys, the dichroism is observed through the different build-up of electronic population. It is pronounced at early delays and is subsequently lost as electrons scatter away from the K points. The build-up and maximum of electronic population are slightly delayed for the circular pump polarization which predominately excites the opposite (K') valleys. This suggests that electronic scattering between the non-equivalent K-valleys is significant and contributes to the rapid reduction of dichroic signal with delay.

The decay of population at the K points is accompanied by an increase of signal at the Σ points, as carriers scatter towards the global minimum of the conduction band. In monolayers, these states are energetically higher, and

directly couple to the substrate[18]. The dynamics of the populations in the Σ valleys are, within our experimental accuracy, independent of pump helicity, despite the dichroic population in the K valleys. This is explained by the different orbital character of states at the Σ valleys, which our DFT calculations predict to be more delocalized between the layers as revealed by the k_z-dispersion shown in Figure 3b.

To obtain a quantitative understanding of the scattering pathways and relative efficiencies, the dynamics of the electronic populations are modelled with a set of rate equations, assuming an initial valley-selective excitation of carriers (see Methods for details). Figure 3c shows the scattering processes included in the model. As states at Σ are delocalized along the z-direction, they equally fill by scattering from K in one layer and K' in the neighbouring layer, making these indistinguishable. By numerically optimizing the parameters to the six measured time-traces (Figure 3a), the dynamics are well reproduced (solid lines) for $\tau_{K\Sigma} = \tau_{K\Sigma'} = (70 \pm 15)$ fs and $\tau_{KK'} = (60 \pm 30)$ fs. The mechanism for this efficient scattering of electrons from the K to the Σ valleys is not ultimately apparent from the experiments. While the time-scale suggests efficient carrier-carrier scattering, intervalley scattering due to collisions with phonons has also been predicted to play an important role in TMDCs[19]. As these scattering processes have been suggested to be spin-conserving[20] in monolayers, and as the conduction band in the Σ valleys show a pronounced spin texture, we suspect a high degree of spin polarization in the conduction band even after completion of the intervalley scattering. The Σ valley populations are long-lived and remain observable up to several tens of picoseconds.
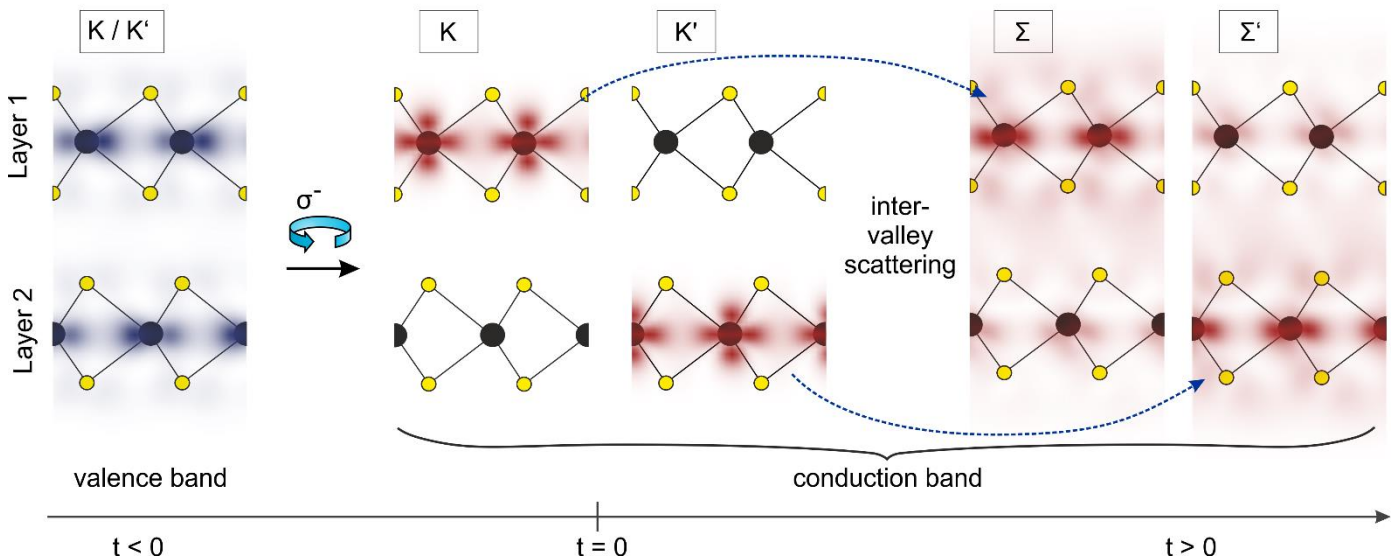

FIGURE 4. Valley- and layer-polarization and spatiotemporal evolution of excited states in a centrosymmetric WSe₂ bilayer. Real space electron densities integrated over one in-plane direction of the wave functions participating in the optical excitation. Left: at t<0, the valence band is occupied at K and K'. Excitation with circularly polarized light populates conduction band states at K and K', but at either point the states are localized in a different layer. This demonstrates the pronounced spin-valley-layer correlation of the excited states arising from the local site asymmetry. Scattering from the K to Σ valleys (dashed blue arrows) in the Brillouin zone occurs on the 100 fs time scale and transforms the excited electrons from 2D to 3D states with pronounced interlayer coupling. In view of utilizing multilayer WSe₂ as source of ultrafast spin currents in heterostructures, efficient electronic coupling of neighbouring layers to the conduction band states at Σ is required.

The key findings of our work are illustrated in Figure 4 by real-space maps of the excited electron density in the conduction band subsequent to spin-selective optical excitation and intervalley scattering. We demonstrate the ability to excite spin-polarized electrons into specific valleys in inversion-symmetric 2H-WSe₂, leading to a valley- and layer-pseudospin polarization, see central panel of Figure 4. These findings are a consequence of atomic site asymmetries[9,11] in TMDCs, and are predicted to occur in a range of materials including topological insulators and superconductors[9]. The ability to project spin texture on excited states in 2H-WSe₂ demonstrates the suitability of nonmagnetic, inversion-symmetric materials for spintronic applications even in the absence of external fields. Our

trARPES study provides a momentum-resolved picture of electronic scattering processes in TMDCs and reveals an efficient scattering from the K to the Σ valleys in the conduction band of WSe$_2$. Our TDDFT calculations show that the excited electrons scatter from pronounced 2D states at K into states with strong 3D character at the minimum of the conduction band (right panel in Figure 4). This suggests a strategy for the extraction of spin-polarized carriers between neighbouring layers in TMDC multilayers and heterostructures[21,22] where the transfer of electrons between layers is governed by the state-dependent interfacial electronic coupling, which can be controlled by an appropriate choice of materials, stacking order and relative orientation. Such control combined with microscopic understanding of electron dynamics as provided here are crucial for conceiving TMDC-based spintronic device concepts.

Methods

trARPES. Time and angle-resolved photoemission (trARPES) experiments were performed at the Materials Science end-station at Artemis (Central Laser Facility, UK), employing fs pump pulses in the visible and probe pulses in the EUV spectral regions at a repetition rate of 1 kHz. An optical parametric amplifier converts the pump-pulses to a central wavelength of 1520 nm. These pulses are then frequency doubled in a BBO crystal to obtain pump pulses of 760 nm central frequency (1.63 eV), slightly above the direct bandgap of WSe$_2$, located at the K-points. A motorized quarter-wave plate is used to change the polarization of the pump pulses.

EUV photons are obtained by high harmonic generation of the fundamental laser pulses in a pulsed argon gas jet. A time-preserving monochromator was used to reduce the obtained spectral width to the 15th harmonic (23 eV photon energy). The energy of the probe photons allows simultaneous measurement of the electronic dynamics at the K (K') and Σ points of the Brillouin zone and ensures maximum sensitivity of the experiment to electrons emitted from the topmost layer. Measurements at the inequivalent K and K' points were performed consecutively after rotating the samples along the K-Γ-K' direction (see Figure 1a). The resulting angle of incidence of the pump and probe pulses on the sample were 15° for measurements at K' and 75° for measurements at K, respectively. The experiments were performed in ultra-high vacuum at room temperature and 80 K (Figure 2b and green triangles in Figure 2c). Single crystals of WSe$_2$ were obtained from HQ Graphene (Netherlands) and cleaved in ultrahigh vacuum prior to measurements. As the cleaving process leads to areas of different surface termination, in the dichroism measurements, the sample surface was scanned for maximum dichroic signal.

DFT Calculations. Band structure calculations of Fig. 1c, 1d and 3b were performed using the ABINIT package[23] within the local spin density approximation[24] and with optimized structural parameters for each geometry. We compare the electronic structure of a bilayer and a six-layer slab and find that the projected electronic structures of the topmost layers for both systems agree well, in particular with respect to the positions of the K and Σ valleys of the CB. For the surface projection, the Kohn-Sham spinor is projected onto the atoms of the top-most layer. The spin polarization is computed by projecting the Kohn-Sham spinor onto the S_z spin operator. The CB states are shifted in energy by 400 meV to match the experimental data The evolution of the electronic structure under pump conditions, Fig. 2d, is computed by propagating the Kohn-Sham equations within TDDFT as provided by the octopus package[25]. The frequency of the pump field was tuned to the gap of the Kohn-Sham states at K. The excited state population is obtained by comparing the time-evolved valence states to the unoccupied states of the ground state. Over time, a growing overlap of a valence state with an unoccupied ground state indicates that the state is assuming the character of an excited state and thus its square modulus is interpreted as the transfer of electronic population to the excited state. All calculations were performed using the HGH pseudopotentials[26].

Scattering Model. The scattering of electrons was simulated by numerically solving a set of rate equations for the excited state populations P_i, with i=K,K',Σ. In the simulations, electronic population is created in the excited state at K, assuming a spin-selective excitation of contrast $c = 0.95$ for circularly polarized and $c = 0.5$ for linearly polarized light. The excitation is taken to be proportional to the intensity of the laser pulse $L(t)$, the shape of which is modeled as a Gaussian function of FWHM 100 fs, close to the experimental conditions. Scattering is assumed to be mono-exponential with rates given as the inverse of the time

constants τ_i. For comparison to the measured intensities I_i, weighting factors M_i are fitted as $I_i = M_i \cdot P_i$ to account for differences of the photoemission matrix elements. Scattering is assumed to be symmetric between K and K', but asymmetric between K/K' and Σ, due to the energetic difference between the two valleys of around 250 meV, which is larger than the maximum phonon energy of around 35 meV[27] and is modelled by the factor α. The set of equations is

$$\frac{\partial P_K}{\partial t} = -\frac{P_K - \alpha \cdot P_\Sigma}{\tau_{K\Sigma}} - \frac{P_K - P_{K'}}{\tau_{KK'}} + c \cdot L(t)$$

$$\frac{\partial P_{K'}}{\partial t} = -\frac{P_{K'} - \alpha \cdot P_\Sigma}{\tau_{K'\Sigma}} + \frac{P_K - P_{K'}}{\tau_{KK'}} + (1-c) \cdot L(t)$$

$$\frac{\partial P_\Sigma}{\partial t} = +\frac{P_K - \alpha \cdot P_\Sigma}{\tau_{K\Sigma}} + \frac{P_{K'} - \alpha \cdot P_\Sigma}{\tau_{K'\Sigma}} - \frac{P_\Sigma}{\tau_{\Sigma d}}.$$

Because of the three-dimensional character of states at the Σ valleys, Σ and Σ' are indistinguishable, such that we take $\tau_{K\Sigma} = \tau_{K\Sigma'} = \tau_{K'\Sigma}$. As electrons in the Σ valleys can scatter away from the surface into the bulk, they are not observed by the experiment, which is accounted for by scattering to unobservable states with time constant $\tau_{\Sigma d}$. The four independent parameters $\tau_{K\Sigma}$, $\tau_{KK'}$, $\tau_{\Sigma d}$ and α of the equations are optimized by a non-linear solver to best reproduce the set of six measured time-traces. Values of τ_i given in the main text and $\alpha = 0.06\pm0.03$ are averages from fitting several datasets, and the given errors are the standard deviation of these values.

References

1. Mak, K. F., He, K., Shan, J. & Heinz, T. F. Control of valley polarization in monolayer MoS2 by optical helicity. *Nat. Nanotechnol.* **7,** 494–498 (2012).
2. Zeng, H., Dai, J., Yao, W., Xiao, D. & Cui, X. Valley polarization in MoS2 monolayers by optical pumping. *Nat. Nanotechnol.* **7,** 490–493 (2012).
3. Gong, Z. *et al.* Magnetoelectric effects and valley-controlled spin quantum gates in transition metal dichalcogenide bilayers. *Nat. Commun.* **4,** 2053 (2013).
4. Xu, X., Yao, W., Xiao, D. & Heinz, T. F. Spin and pseudospins in layered transition metal dichalcogenides. *Nat. Phys.* **10,** 343–350 (2014).
5. Zhu, Z. Y., Cheng, Y. C. & Schwingenschlögl, U. Giant spin-orbit-induced spin splitting in two-dimensional transition-metal dichalcogenide semiconductors. *Phys. Rev. B* **84,** 153402 (2011).
6. Xiao, D., Liu, G.-B., Feng, W., Xu, X. & Yao, W. Coupled Spin and Valley Physics in Monolayers of MoS2 and Other Group-VI Dichalcogenides. *Phys. Rev. Lett.* **108,** 196802 (2012).
7. Cao, T. *et al.* Valley-selective circular dichroism of monolayer molybdenum disulphide. *Nat. Commun.* **3,** 887 (2012).
8. Berghaeuser, G. & Malic, E. Analytical approach to excitonic properties of MoS2. *Phys. Rev. B* **89,** 125309 (2014).
9. Zhang, X., Liu, Q., Luo, J.-W., Freeman, A. J. & Zunger, A. Hidden spin polarization in inversion-symmetric bulk crystals. *Nat. Phys.* **10,** 387–393 (2014).
10. Yu, S.-W. *et al.* Spin resolved photoemission spectroscopy on WSe2. *J. Electron Spectros. Relat. Phenomena* **101-103,** 449–454 (1999).
11. Riley, J. M. *et al.* Direct observation of spin-polarized bulk in an semiconductor bulk inversion-symmetric semiconductor. *Nat. Phys.* **10,** 835–839 (2014).
12. Runge, E. & Gross, E. K. U. Density-Functional Theory for Time-Dependent Systems. *Phys. Rev. Lett.* **52,** 997–1000 (1984).
13. Finteis, T. *et al.* Occupied and unoccupied electronic band structure of WSe2. *Phys. Rev. B* **55,** 10400–10411 (1997).
14. Jones, A. M. *et al.* Spin–layer locking effects in optical orientation of exciton spin in bilayer WSe2. *Nat. Phys.* **10,** 130–134 (2014).
15. Riley, J. M. *et al.* Negative electronic compressibility and tunable spin splitting in WSe 2. *Nat. Nanotechnol.* **10,** 1–6 (2015).
16. Frindt, R. F. The optical properties of single crystals of WSe2 and MoTe2. *J. Phys. Chem. Solids* **24,** 1107–1108 (1963).
17. Chernikov, A., Ruppert, C., Hill, H. M., Rigosi, A. F. & Heinz, T. F. Population inversion and giant bandgap renormalization in atomically thin WS2 layers. *Nat. Photonics* **9,** 466–471 (2015).
18. Grubišić Čabo, A. *et al.* Observation of Ultrafast Free Carrier Dynamics in Single Layer MoS2. *Nano Lett.* **15,** 5883–5887 (2015).
19. Steinhoff, A. *et al.* Nonequilibrium Carrier Dynamics in Transition Metal Dichalcogenide Semiconductors. *arXiv Prepr. arXiv1603.03633* (2016).
20. Liu, H. J. *et al.* Observation of intervalley quantum interference in epitaxial monolayer tungsten diselenide. *Nat. Commun.* **6,** 8180 (2015).

21. Geim, A. K. & Grigorieva, I. V. Van der Waals heterostructures. *Nature* **499,** 419–425 (2013).
22. Withers, F. *et al.* Light-emitting diodes by band-structure engineering in van der Waals heterostructures. *Nat. Mater.* **14,** 301–306 (2015).
23. Gonze, X. *et al.* ABINIT: First-principles approach to material and nanosystem properties. *Comput. Phys. Commun.* **180,** 2582–2615 (2009).
24. Perdew, J. P. Self-interaction correction to density-functional approximations for many-electron systems. *Phys. Rev. B* **23,** 5048–5079 (1981).
25. Andrade, X. *et al.* Real-space grids and the Octopus code as tools for the development of new simulation approaches for electronic systems. *Phys. Chem. Chem. Phys.* **17,** 31371 (2015).
26. Hartwigsen, C., Goedecker, S. & Hutter, J. Relativistic separable dual-space Gaussian pseudopotentials from H to Rn. *Phys. Rev. B* **58,** 3641–3662 (1998).
27. Sahin, H. *et al.* Anomalous Raman spectra and thickness-dependent electronic properties of WSe2. *Phys. Rev. B* **87,** 165409 (2013).

Acknowledgments

Author Contributions

R.B. and R.E. conceived the study. R.B., C.W.N., C.M., L.W., C.C. and R.E. conducted the experiments. C.C., R.T.C. and E.S. managed the facility, developed the instrumentation and provided technical support for the beamline. H.H. and U.G. performed the DFT calculations. R.B., C.W.N. and L.W. analysed the data. L.W., R.B., C.W.N., H.H. and R.E. wrote the manuscript. All authors contributed to the interpretation of the results and commented on the manuscript.